Why do inverse eddy surface temperature anomalies emerge ? The case of the Mediterranean Sea

Evangelos Moschos[1], Alexandre Barboni[1], Alexandre Stegner[1]

[1]Laboratoire de Météorologie Dynamique, Ecole Polytechnique, 91128 Palaiseau, France

Key Points:

- The the emergence of inverse Cold Anticyclones and Warm Cyclones is a seasonal phenomenon that affects the life cycle of mesoscale eddies.
- The core temperature anomaly of eddies is characterised with a simple index, showing that 70% of their signatures are inverse in Mediterranean summer.
- Vertical mixing modulation by mesoscale eddies might be the key mechanism that leads to the emergence of inverse eddy signatures.

Corresponding author: Evangelos Moschos, `evangelos.moschos@polytechnique.edu`

Abstract

It is widely accepted that the signature of anticyclonic (cyclonic) eddies on the sea surface temperature corresponds to a warm (cold) core anomaly. Nevertheless, this statement has been put to question by recent regional studies showing the existence of inverse eddy SST anomalies: cold-core anticyclones and respectively warm-core cyclones. This study shows that the emergence of these inverse signatures is a seasonal phenomenon that affects the life cycle of mesoscale eddies in the Mediterranean Sea. We use remote-sensing observations and in-situ data to analyse the eddy-induced SST anomaly over a 2 years period (2016-2018). We build an eddy core surface temperature index to quantify the amount of Cold Core Anticyclones and Warm Core Cyclones all over the year and especially during the spring re-stratification period. We find that these inverse eddy signatures could reach a peak of 70% in May and June, both for cyclones and anticyclones. Besides, in order to understand the underlying dynamical processes, we construct a simple vertical column model to study the impact of the seasonal air-sea fluxes on the surface stratification inside and outside eddies. It is only by taking into account a differential diapycnal eddy mixing - increased in anticyclones and reduced in cyclones - that we reproduce correctly, in agreement with the observations, the surface temperature inversion in the eddy core. This simplified model, suggests that vertical mixing modulation by mesoscale eddies might be the key mechanism that leads to the eddy-SSTA seasonal inversion in the ocean.

Plain Language Summary

Mesoscale eddies, swirling ocean circulations with scales of less than 100km, distinguished in anticyclones and cyclones based on their pressure anomaly and sense of rotation. It is widely accepted that anticyclones are warm eddies, while cyclones are cold ones. In this study we analyze the visible signature of eddies on Sea Surface Temperature images in the Mediterranean Sea, and find that inverse signatures, that is cold anticyclones and warm cyclones, are omnipresent and their emergence peaks in summer. To explain these signatures we propose a simple mechanism which considers the vertical oceanic mixing induced by eddies, and reproduces the emergence of these inverse anomalies.

1 Introduction

Mesoscale eddies are coherent structures with radii equal or larger than the local Rossby deformation radius. These eddies are usually long-lived and they can survive several months or even years. Significant advances in the resolution of both satellite altimetry measurements (Chelton et al., 2011) and high resolution oceanic numerical models (Su et al., 2018) have revealed the predominance of these mesoscale eddies in the global oceanic circulation. They are able to trap and transport heat, salt, pollutants and various biogeochemical components from their regions of formation to remote areas (Zhang et al., 2014; Laxenaire et al., 2018). Their dynamics can impact significantly the biological productivity at the ocean surface (Gaube et al., 2013; McGillicuddy Jr, 2016; Lévy et al., 2018), modify the depth of the mixed layer (Gaube et al., 2019), influence clouds and rainfall within their vicinity (Frenger et al., 2013), amplify locally the vertical motions (Klein & Lapeyre, 2009), attract pelagic species (Baudena et al., 2021; Abrahms et al., 2018; Gómez et al., 2020) or concentrate and transport micro-plastics (Brach et al., 2018). Hence, long-lived mesoscale eddies play a prominent role in ocean circulation differentiating from the mean patterns in various regions such as the Southern Ocean (Mazloff et al., 2010), the Sargasso Sea (McGillicuddy et al., 1998), the Indo-Atlantic exchange (Laxenaire et al., 2018, 2019, 2020) or the Mediterranean Sea (Hamad et al., 2006; Amitai et al., 2010; Menna et al., 2012; Mkhinini et al., 2014; Escudier et al., 2016; Ioannou et al., 2017; Pessini et al., 2018; Barboni et al., 2021). This study is focused on the latter.

The use of infrared images, which measure the Sea Surface Temperature (SST), since the early 80's, has allowed the detection of many oceanic eddies and a better understanding of regional circulations (Millot, 1985; Auer, 1987; Hamad et al., 2006). These detections were performed visually by expert oceanographers. However, due to the scarcity of in-situ observations, it was not until the intensive development of satellite altimetry and the first automatic vortex detection algorithms on the Sea Surface Height (SSH) fields that a statistical link between Eddy-induced Sea Surface Temperature Anomalies (eddy-SSTA) and SSH anomalies was established. Early studies such as (Hausmann & Czaja, 2012) used composites of eddy-SSTA, deriving that anticyclones (respectively cyclones) are associated with warm (cold) eddy-SSTA. In the same manner Frenger et al. (2013) and Gaube et al. (2015) linked the mean composite signature of SST anomalies in the eddy vicinity with modulation of wind, rainfall and cloud coverage conditions.

This association of warm eddy-SSTA with anticyclones and cold ones with cyclones, present in a large part of the bibliography, has been put to question by various regional studies showing the existence of inverse eddy-SSTA signatures i.e. anticyclones (respectively cyclones) with cold (warm) core signature. As soon as in the early 2000's Hamad et al. (2006) already performed observations of some cold core anticyclones on the summer period in the Eastern Mediterranean sea, proposing an explanation of their formation through the advection of surface colder waters stemming from higher latitudes. Everett et al. (2012) observed the existence of an important fraction (70%) of inverse signatures in the Tasman Sea eddy avenue. Leyba et al. (2017) found cyclones with a warm eddy-SSTA in the southwestern Atlantic ocean, which are explained through their (warm) region of formation. Trott et al. (2019) showed the existence of inverse signatures in the Arabian Sea, while searching for a link between the SST and MLD anomaly. Sun et al. (2019) performed similar observations in the North Pacific Ocean, and also showed a seasonal variability in the regional eddy temperature anomaly distribution, noting that these inverse signatures appear for shorter times than the regular ones. In the same fashion, Liu et al. (2020) analysed the inverse eddy-SSTA in the South China Sea and noted a slight dependence on both seasonal effects and eddy amplitude. The last two studies, both link inverse signatures with the summer re-stratification at the ocean surface.

The omnipresence of cold-core anticyclonic and warm-core cyclonic eddies around the globe has been documented by two recent studies. Through a Deep Learning eddy identification method based on semantic segmentation, Liu et al. (2020) detected and classified eddies and their surface temperature anomaly. An important fraction of inverse signatures is revealed around the globe, reaching up to 40%. The authors also showcase the seasonal variation of this fraction as well as an interannual trend of diminishing inverse signatures. In the same manner Ni et al. (2021), showcases that inverse signature eddies have lower SST anomaly values than their regular counterparts. Exhibiting strong seasonal variation, inverse signatures cover according to this paper as much as 15% of anticyclones (10% cyclones) on summer period. Finally the authors show correlation of this seasonal variation of eddy SST anomalies with the mixed layer modulation, along with the inversement of wind-stress and heat-flux patterns over these eddies.

However, correlation does not imply causation, and even if some of the aforementioned articles create a strong observational link, regionally or globally, between the mixed

layer modulation and the inversion of eddy-SSTA signatures, none of them demonstrates an underlying mechanism for this phenomenon.

The goal of this work is to perform a comprehensive study on the formation of inverse sea surface temperature anomaly of mesoscale eddies, and propose an underlying physical mechanism. As a case study, observations in the Mediterranean Sea are examined, although our results can be expanded to other regions of the globe. Here, we attempt to answer four questions:

- *How does the eddy-SSTA distribution vary seasonally? :* We first define an eddy core surface temperature anomaly index to quantify the intensity of the eddy-SSTA for a large number of cyclonic and anticyclonic eddies in the Med Sea. This index allows us to perform a statistical analysis of the seasonal variations of the temperature anomaly inside coherent eddies and study its correlation with the evolution of the mixed layer depth.

- *How does the SST signature of an individual mesoscale structure evolve? :* We investigate a few long-lived eddies to follow the temporal evolution of their SST signature with respect to their dynamical parameters and the seasonal stratification of the ocean surface.

- *Is the surface temperature signature linked with the subsurface structure? :* We quantify more precisely the evolution of the surface stratification inside and outside these selected eddies using ARGO profiles to estimate the eddy vertical temperature structure and compare it with the surface temperature anomaly.

- **Why do inverse SST signatures emerge? :** We propose a mechanism based on differential vertical mixing between the eddy core and its periphery under atmospheric fluxes, illustrated with idealized single-column numerical simulations. The relevance of this physical model to explain the inverse emergence of inverse eddy-SSTA and its agreement with the remote-sensing and in-situ observations are discussed in the conclusion.

2 Satellite and in-situ data

This study focus on the mesoscale oceanic eddies of the Mediterranean Sea, during the three-year period 2016-2018. To perform our analysis, we combine satellite and in-situ data to characterize both the ocean surface and the subsurface stratification. The

infrared satellite imagery provides the Sea Surface Temperature (SST) maps which are the core data of this study. We use the DYNED-Atlas database to obtain the dynamical parameters and the contours of mesoscale eddies detected on standard satellite altimetry products. The three dimensional structures of the studied eddies, as well as the surface stratification and the mixed layer depth (MLD) were derived from the in-situ Argo floats measurements.

2.1 Satellite Data

Daily, high-resolution (1/120°) super-collated SST maps of the Mediterranean Sea are received from the Copernicus - Marine Environment Monitoring Service (CMEMS), Ultra High Resolution L3S SST Dataset, produced by the CNR - Italy and distributed by CMEMS. The process of supercollation uses SST measurements derived from multiple sensors, representative of nighttime SST values (Nardelli et al., 2013).

Sea Surface Height (SSH) and geostrophic velocity fields, used in Figures of this study, are L4 altimetric products at 1/8°resolution retrieved from the CMEMS L4 Sea Level dataset.

2.2 Eddy contours, centers and tracks

The dynamical evolution of eddies and their individual tracks are retrieved from the DYNED-Atlas database for the three year period 2016-2018. The DYNED-Atlas project containing eddy tracks and their physical properties is publicly accessible . The tracking of these eddies is performed by the AMEDA eddy detection algorithm (Le Vu et al., 2018) applied on daily surface velocity fields, derived from the aforementioned SSH maps. A cyclostrophic correction is applied on these geostrophic velocities to accurately quantify eddy dynamical properties (Ioannou et al., 2019). Unlike standard eddy detection and tracking algorithms, the main advantage of the AMEDA algorithm is that it detects the merging and the splitting events and allows thus for a dynamical tracking of eddies (Le Vu et al., 2018).

The identification of potential eddy centers by AMEDA is performed by computing the Local Normalized Angular Momentum (LNAM) (Mkhinini et al., 2014) of the geostrophic velocity field. Only eddy centers with at least one closed contour of the stream function of the velocity field are retained. A radial profile of the velocity for each detected

eddy center is calculated by computing the average velocity and radius at each closed streamline around it:

$$\langle V \rangle = \frac{1}{L_p} \oint \vec{V} \, d\vec{l} \tag{1}$$

$$\langle R \rangle = \sqrt{\frac{A}{\pi}} \tag{2}$$

The maximum velocity, obtained through equation 1, will be hereby noted as V_{max} and the radius corresponding to this characteristic contour, obtained through equation 2, will be noted as R_{max}. The eddy centers and their characteristic radius R_{max} are important parameters used to retrieve SST patches for each eddy detection.

2.3 Argo Floats

Hydrographic profiles of Argo floats are received through the CORIOLIS program database. Potential temperature and salinity profiles are received from Argo floats, through which the potential density profiles are derived. A co-localization is performed between the position of Argo floats and the detected eddies of the DYNED-Atlas database. Argo profiles are marked as inside an eddy if their distance r from any eddy center is $r < R_{max}$ and outside an eddy if the above condition is false for every eddy detection of the same day.

To calculate the Mixed Layer Depth (MLD) of each Argo observation, we use its potential density profile and search for the maximum depth at which a threshold of $\delta\rho = 0.02 kg/m^3$ is reached.

3 Quantifying eddy-induced SST anomalies

Mesoscale eddies often have a visible signature on SST images, with a temperature difference between the waters in the eddy core and the waters in its periphery. This difference is hereby referred to as the eddy-induced surface temperature anomaly (eddy-SSTA) of an eddy, and can be quantified through our proposed methods.

A procedure to retrieve a large dataset of SST image patches containing eddy signatures is proposed, following Moschos, Schwander, et al. (2020); Moschos, Stegner, et al. (2020). The Eddy-Core Surface Temperature Anomaly Index (δT), a simple and heuristic method for quantifying the eddy-induced temperature anomaly represented in each

image, is then defined. The proposed methodology, applied here to observations in the Mediterranean Sea, is generic enough to provide results in every oceanic domain.

3.1 Eddy SST patches dataset

A thorough statistical analysis of eddy-induced SST anomalies requires a large data set of SST image patches in the Mediterranean Sea. The characteristic contours (highest mean velocity) of the mesoscale eddies contained in the DYNED-Atlas are used to crop patches from SST maps, centered on the detected eddies. These contours can either represent Anticyclonic Eddies (AE) or Cyclonic Eddies (CE) rotating clockwise and anti-clockwise respectively in the northern hemisphere. For each eddy, a square patch of size $(5R_{max}{\times}5R_{max})$ is cropped, centered on the contour barycenter. Cloud coverage creates missing values on satellite SST images, and can corrupt the signature of the cropped image patches. Thus, only patches with less than 50% of cloudy pixels are retained. All the SST patches are then interpolated to a constant pixel size (224x224), through a nearest neighbour method.

As shown in the previous studies, the SST eddy signatures can be distinguished either as Warm-Core (WC) or Cold-Core (CC) anomalies. Four such cases are depicted in Figure 1 that both positive and negative SSH anomalies can correspond to a Warm or a Cold SST signature. The characteristic contour of each eddy (in black) are superimposed on the Absolute Dynamic Topography (ADT), derived from the SSH, and the corresponding SST patch.

3.2 The Eddy-Core Surface Temperature Anomaly Index [δT]

The Eddy-Core Surface Temperature Anomaly Index (hereby δT) is a simple and heuristic metric of the temperature difference between the core (center) of the eddy and its periphery. The value of δT is calculated as the difference between the mean of the temperature values inside a *core-mean frame* and a *periphery-mean frame* in a given patch, with units in $°C$. These two square frames, which share a common center, have sides of $\frac{2}{3}R_{max}$ and $4R_{max}$, respectively. For the calculation of the mean value in the periphery-mean frame, the values contained in the core-mean frame are ignored. A positive δT value denotes a larger core-mean temperature than its periphery-mean temperature and thus a Warm Core Eddy, while a negative δT denotes respectively a Cold Core Eddy. The
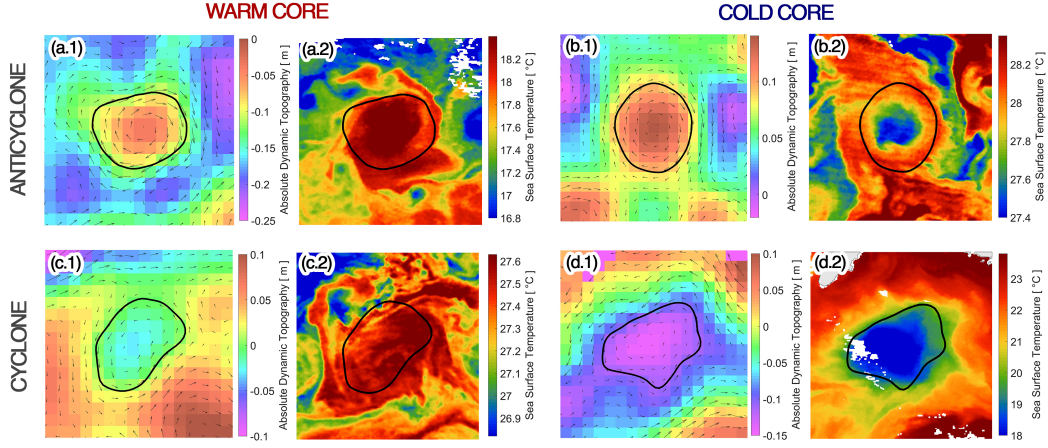
Figure 1. **Samples of eddy induced SST anomalies** for a **(a)** Warm-Core Anticyclone, **(b)** Cold-Core Anticyclone, **(c)** Warm-Core Cyclone, **(d)** Cold-Core Cyclone. On the leftmost panels numbered with **(1)** the velocity vectors and the characteristic contour, computed by the AMEDA algorithm (black line) are superimposed on the Absolute Dynamic Topography. On the rightmost panels numbered with **(2)** the characteristic contour (black line) are superimposed on the patches of Sea Surface Temperature field centered on the detected eddy. Image patches are of side $5R_{max}$.

calculation of the δT variable by use of the core-mean and periphery-mean frames is shown in Figure 2. Examples (a) and (b) show the two centered signatures, shown also in Figure 1 (a.2) and (b.2). The δT values are $0.75°C$ for the WC example (a) and $-0.27°C$ for the CC example (b).

However, the barycenter of the velocity contour can differ from the center of the eddy SST anomaly core, due to bias or errors of altimetric maps (Amores et al., 2018; Stegner et al., 2021). Therefore, an offset of both frames is considered, in order to locate the exact position of the maximum eddy-SSTA and correct the index value.

This correction is computed as follows: First, the value of δT is calculated through squares centered on the image, as described above. The sign of the eddy-induced SST anomaly is thus defined. Then, if δT is positive (negative) the warmest (coldest) core-mean value is searched for, by offsetting the core-mean frame in all directions with a stride of $\frac{1}{9}R$ and a maximum offset of $\frac{2}{3}R$. Finally, the periphery-mean frame is centered along the shifted core-mean frame and the corrected δT value is computed. In the rest of this manuscript δT represents the final values calculated by applying the offset correction.

Examples of off-centered eddy detections are shown in Figure 2 (c) and (d). The core and periphery have been shifted in order to maximize the eddy-core surface temperature anomaly index. The geometric center of the image is shown with a white cross, while the shifted center of the core-mean frame is shown with a yellow cross. The δT values are $0.68°C$ corrected to $0.86°C$ by offseting, for the WC example (c) and $-0.46°C$ corrected to $-0.55°C$ by offseting for the CC example (d).

Nevertheless, even with this correction a significant amount of noisy and/or corrupted SST signatures remain. This could be due to the combination of erroneous eddy detections on gridded AVISO/CMEMS altimetry products, large scale air-sea interactions that mask mesoscale eddy signature or the presence of clouds (Moschos, Stegner, et al., 2020).

In order to exclude these images with unclear SST signatures, two thresholds are considered. The Cloud Coverage threshold, described above is used to retain only im-
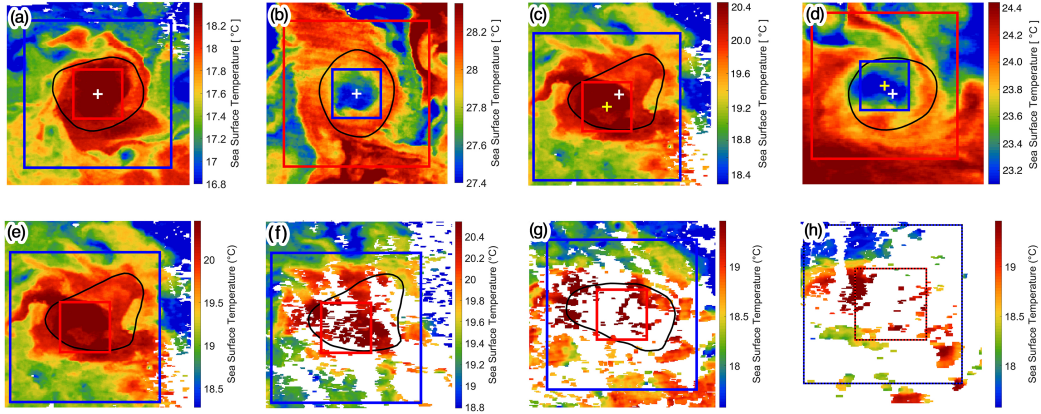
Figure 2. **Examples of the Eddy-Core Surface Temperature Anomaly computation method.**. Snapshots represent Sea Surface Temperature in degrees. Black lines are superimposed altimetric detection contours. Small squares represent the core-mean and large ones the periphery-mean frames. Core-periphery are coloured red-blue or blue-red based on the sign of δT. Examples (a)-(d) illustrate the correction by offset: A white cross marks the center of the image. A yellow cross marks the center of the core-mean and periphery-mean frames, if it differs from the center of the image. Examples (a) and (b) are centered while (c) and (d) are offseted. Examples (e)-(f) illustrate the filtering by cloud coverage. Examples (e) and (f) are retained while (g) and (h) are filtered.

ages that contain less than 50% of cloudy pixels. This criterion is applied twice: on the whole image patch (CCP_{patch}), as well as the core-mean frame (CCP_{frame}).

An illustration of the application of the Cloud Coverage threshold is provided in Figure 2 (e)-(h), where snapshots of the SST signature of the same eddy are provided at different days, along with core-mean and periphery-mean frames. Example (a) shows a patch with an overly clear eddy signature ($CCP_{patch} = 8\%, CCP_{frame} = 0\%$), retained in the dataset. Example (b) shows a patch with an eddy signature covered by clouds ($CCP_{patch} = 40\%, CCP_{frame} = 48\%$), which however do not surpass the 50% threshold and is retained in the dataset. Examples (c) ($CCP_{patch} = 48\%, CCP_{frame} = 90\%$) and (d) ($CCP_{patch} = 72\%, CCP_{frame} = 76\%$) show patches exceeding the Cloud Coverage threshold and therefore filtered from the dataset.

Finally a filter on weak δT values is also applied. We have noticed by visual inspection that unclear SST signatures often induce a week value of the δT. Hence, to filter out these noisy images we retain only SST patches if $|\delta T| > 0.1$.

## 4 Seasonal variations of the eddy-induced temperature anomaly

4.1 Statistical viewpoint

Composite averages are often employed in the bibliography to represent the SST signature of mesoscale eddies. This averaging leads frequently to the association of a warm-core signature to anticyclonic eddies and a cold-core signature to cyclonic eddies.

To examinate these average temperature anomalies we calculate here the composites of all eddy SST patches retained, after first performing a normalization per patch. To receive the Normalized SST Anomaly, we substract from each pixel the mean value of all the patch pixels and divide the result by the standard deviation of all the patch pixels. In Figure 3 composites of Anticyclonic and Cyclonic Normalized SST Anomaly are plotted for all eddies and those observed on the Winter (December-January-February) and Summer (May-June-July) period. These two oceanic seasons are chosen on the three months period when the mean value of the mixed layer depth (MLD), computed outside the detected eddies, reaches its largest or smallest value (see Figure 5).

From the composites of Figure 3 it can be seen that the average signature of all anticyclonic (cyclonic) observations indeed corresponds to a warm-core (cold-core) struc-
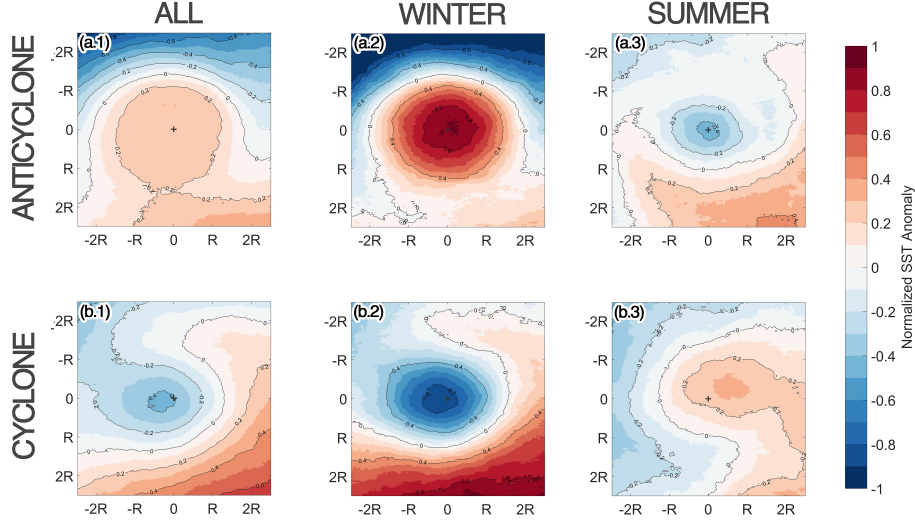
Figure 3. **Composite averages of Normalized SST Anomaly** for (a) Anticyclonic and (b) Cyclonic eddies, for (1) all (2) winter (DJF) and (3) summer (MJJ) observations. Each value in an eddy SST patch is normalized by subtracting the mean value and dividing by the standard deviation of all values. Composites are retained by averaging between patches.

ture, or else the regular eddy signature. Nevertheless, a strong seasonal variation of this average signature is revealed by plotting the winter and summer composites. On winter, the regular signature is even more pronounced with double to triple normalized anomaly values. On summer, the average signature is inversed with a weaker however normalized anomaly values.

While composites suffice to portray the seasonal inversion of eddy temperature anomaly signatures, averaging out patch values looses the information on the variability of the signal. To quantify thus the latter we perform a statistical analysis of the δT index values computed for all the patches retained.

The histograms of the δT index are shown in Figure 4, separately for anticyclonic and cyclonic eddies, at winter (DJF) and summer (MJJ). On the histograms, red bins represent warm-core observations, while blue bins represent cold-core observations. Grey bins represent observations where $|\delta T| < 0.1$, which are filtered due to a weak eddy-SSTA.

If we consider a year-long statistical distribution, AE are predominantly Warm Core and CE are predominantly Cold Core, in other words AE and CE, exhibit on average

a *regular* signature on the SST. However, the distribution of δT values in the histograms of Figure 4 suggest that the eddy-core temperature anomaly exhibits strong seasonal variation, altering between Warm Core and Cold Core anomaly regimes. Specifically, during winter the regular signatures are preponderant: 93% of AE observations correspond to Warm Core eddy and while 92% of CE observations being Cold Core. However, during summer, Cold Core AE and Warm Core CE observations become dominant with respectively 69% and 66% of the observations. It is due to this seasonal inversion of the regular signature, that we name the Cold Core AE and Warm Core CE as *inverse* SST signature.
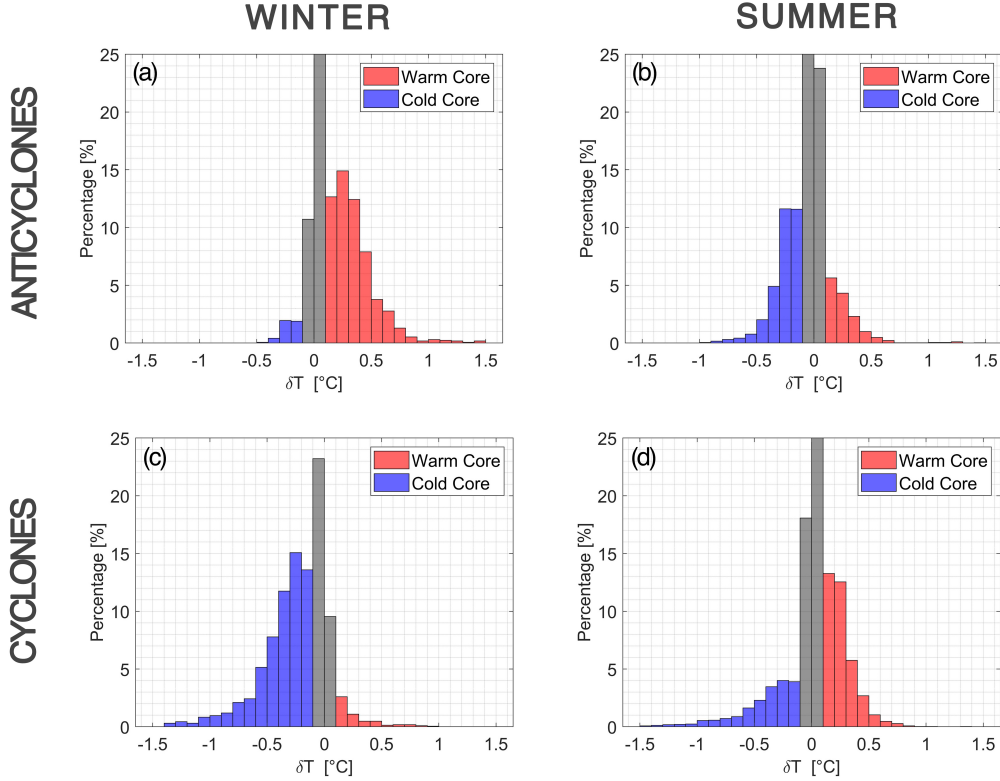
Figure 4. **Seasonal histograms of δT values**. **(a)** AE in the winter mixing period (DJF), **(b)** AE in the summer restratification period (MJJ), **(c)** CE in the winter mixing period (DJF) and **(d)** CE in the summer restratification period (MJJ). Red bins represent positive δT warm-core observations while blue bins negative δT cold-core observations. Grey bins represent observations where $|\delta T| < 0.1$.

The seasonal cycle of the eddy-SSTA of both AE and CE, in the Mediterranean Sea, coincides with the seasonal variation of the Mixed Layer Depth (MLD). This is portrayed in Figure 5, were the monthly variation of the percentage of inverse eddy core signatures is plotted along with the monthly variation of the MLD. The later is calculated as the mean of all Argo profiles that are located outside eddies. The winter mixing period (DJF) when the mean MLD is at its largest extent, coincides with the period when inverse signatures appear with the lowest percentage between 5−15% for both AE and CE. Conversely, the end of the spring re-stratification period (MJJ) when the mean MLD is at its shallowest, coincides with the period when inverse signatures appear at their highest percentage, reaching a peak of 70% of cold-core AE and warm-core CE observations for the months of May and June.
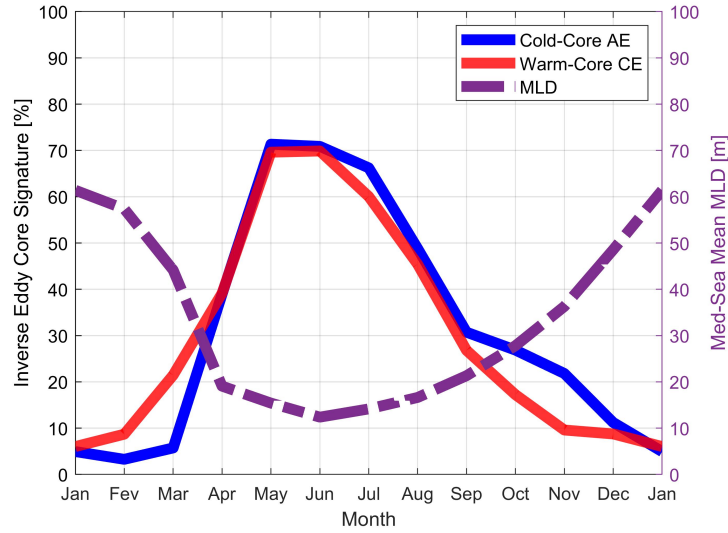
Figure 5. **Seasonal variation of the Mean MLD with inverse eddy signature percentage.** For each month the mean percentage of Cold-Core AE observations is plotted with a blue line, the mean percentage of Warm-Core CE observations with a red line and the mean MLD of all Argo profiles located outside eddies with a dashed purple line.

4.2 Individual eddy viewpoint

To better investigate how the seasonal evolution of the surface stratification inside mesoscale eddies impacts their surface signatures, we track four long-lived eddies and followed the temporal evolution of their dynamical parameters, the surrounding MLD

and their surface signature. One of them, an Ierapetra Anticyclone, formed south of the island of Crete, was sampled for over a year by a few Argo floats trapped inside its core. Three more eddies are considered: a Cyprus anticyclone located among and around the Eratosthenes seamount, an Algerian Anticyclone drifting along the Algerian coast and an elongated cyclone located in the Ligurian sea.

For each of these four eddies we create an *Eddy Timeline*, that contains the δT index, the evolution of the mixed layer depth (MLD) in the eddy area, the eddy intensity and a few characteristic snapshots of the eddy SST signature. Moreover, to highlight the seasonal variations a monthly mean average (MMA) is calculated for each parameter. The daily value of the Core Temperature Anomaly Index (δT), are plotted when the cloud coverage is not too high and the temperature anomaly not too small (i.e. $|\delta T| > 0.1$). The calculated (δT) (dots) as well as the corresponding MMA (line) are coloured in red (blue), when their value is positive (negative), denoting a warm (cold) core regime.

To construct the MLD time series (pink dots), we use all the Argo profiles that were measured outside the eddy contour in a surrounding area, defined as a rectangular box of one degree of latitude and longitude, centered on the eddy. More than one MLD observation might exist for a certain day, causing a spread of values especially for the winter mixing period. When in-situ measurement are available inside the eddy contour, the MLD is plotted with black dots. The variations of the eddy intensity, quantified here by V_{max}, is plotted during the same period. In order to highlight the seasonal variations, we use distinct colors for the velocity above (magenta) and below (cyan) the mean velocity value averaged over the whole period.

Our analysis is focused on the evolution of an Ierapetra Anticyclone from September 2016 to September 2018. According to the figure 6, this anticyclone changes regime twice from a regular to an inverse signature. The inverse sea surface temperature anomaly begins in spring, when the re-stratification sets in, and continues until fall.
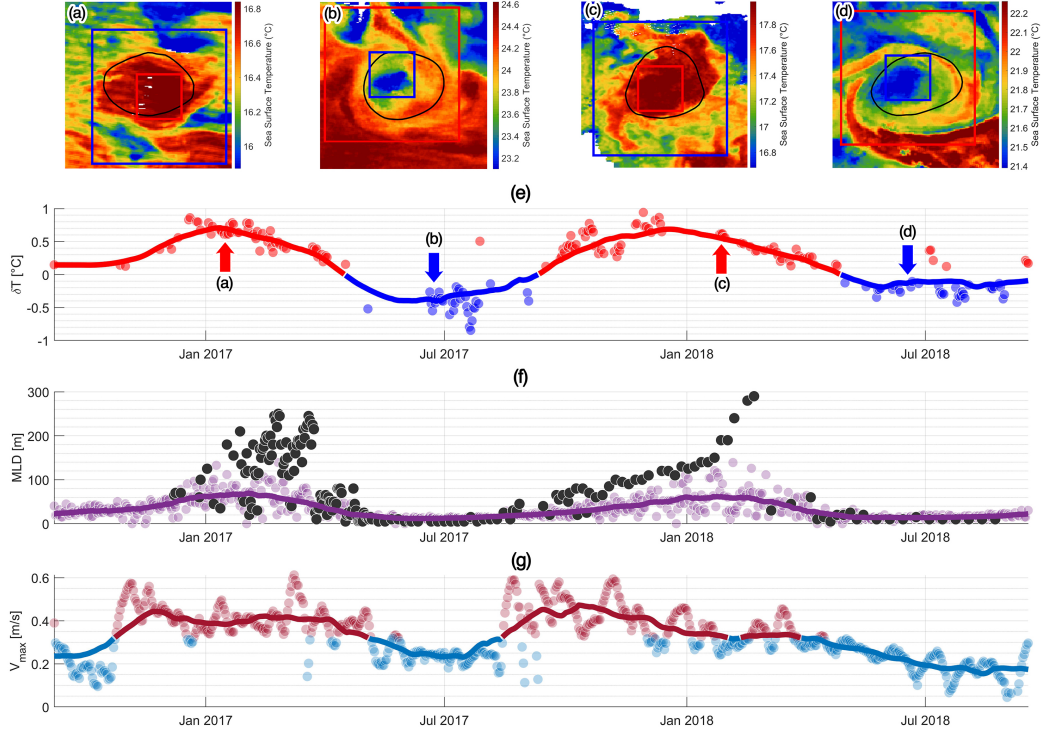
Figure 6. **Timeline of the Ierapetra Anticyclone** with DYNED ID #11099. Four characteristic SST patches are shown in panels (a)-(d) which corresponds to different regimes of the evolution of the eddy SST anomaly, shown in panel (e): the δT index values are plotted for every retained observation with red (blue) dots for positive (negative) values. The MMA of these values is plotted with a red (blue) line showing the regime change between a warm-core (cold-core) eddy. On panel (f) the depth of the mixed layer (MLD) is plotted with pink dots for values outside the eddy and black dots inside the ierapetra eddy. A MMA of the MLD evolution outside the eddy is plotted with a pink line. On panel (g) the surface maximal velocities (V_{max}) for each timestep in the DYNED-Atlas eddy track are plotted with dots and their MMA with a line. Velocities are plotted with magenta (cyan) when they are higher (lower) than the mean velocity in the eddy lifetime.

As can be seen in panel (f) of Figure 6, on winter months, while the eddy is a warm-core regime in panel (e), the MLD is two or three times deeper inside the ierapetra anticyclone than in its surroundings, reaching 300 meters of depth while being shallower than 120 meters in its surroundings. The warm-core surface signature of the eddy (panels (a) and (c)) can be linked therefore with its subsurface heat content. On the other hand, during the spring re-stratification period and a cold-core regime, the MLD is rather

shallow, not exceeding a few tens of meters both inside and outside the anticyclone. The cold-core surface signature (panels (b) and (d)) is disconnected from the warm subsurface heat content. It should also be noted, that it is during the winter months, when the MLD is deeper in the eddy core, that the anticyclone passes an intensification phase shown in the evolution of the surface velocity V_{max}.

Similar regime transitions from a regular to an inverse sea surface temperature anomaly are visualized in the supplementary material of this article for a cyclonic eddy in Figure S1 as well as for two other anticyclones in Figures S2 and S3. For all these eddies the inverse sea surface temperature anomaly, is directly correlated to a small MLD in the eddy surrounding. This indicates a strong surface stratification on the same period and thus a disconnection of the inverse surface signature with the subsurface heat content.

To investigate if the change in the surface core temperature anomaly is linked with the subsurface anomaly of the Ierapetra anticyclone two profiles from an ARGO float released inside the core of the eddy are examined. From a series of observations, the profiles are chosen on two dates where the SST signature of the eddy is not corrupted by clouds and the in-situ profile samples well the eddy core. On winter a regular warm-core observation, on the 26 February 2017 can be seen in panel (a.2) of Figure 7, corresponding to panel (a) of Figure 6. On summer a regular warm-core observation, on the 26 of June 2017 can be seen in panel (b.2) of Figure 7, corresponding to panel (b) of Figure 6. On these panels a white star corresponds to the location of the eddy-sampling ARGO float. On panels (a.1) and (b.1) of Figure 6 the location of the eddy-sampling floats are shown with a star in a wider map, where we also plot the region (dashed rectangle) where we search for background-sampling ARGO floats. We consider a ± 1 week period from the observation date and search for ARGO profiles in that region that fall outside of eddies. The temperature measurement of these background outside-eddy profiles is plotted with dashed gray lines on panels (c) and (d) of Figure 6 while their mean is plotted with a thick black line. The eddy-sampling profile is plotted on panels (c) and (d) of Figure 6 corresponding to the winter and summer periods respectively. When eddy-sampling profile is warmer (cooler) than the mean outside-eddy profile it is plotted with a thick red (blue) line.

Due to the deep winter mixed layer, the warm core SSTA extends down to 250m (Fig.7 (c)). On this winter profile, the core of the anticyclone is always warmer that its

surrounding down to 1000m. An inversion of the eddy-SSTA is visible on the summer profile (Fig.7 (d)). However this cold core temperature anomaly does not extend below a few tens of meters (Fig 7 (e)). Below the strong summer stratification, at -100m for instance, the core temperature of the anticyclone is warmer than its surrounding waters whose temperature is portrayed by the mean outside-eddy profile (black line in Figure 7 (d)). The subsurface temperature anomaly reaches a positive value of $+1°C$ at 500m, which is coherent with other observations of long-lived anticyclonic eddies in the region (Moutin & Prieur, 2012; Barboni et al., 2021). Hence, these unique in-situ measurements indicate that the inverse eddy-SSTA remains confined to a few dozen meters below the ocean surface and does not correspond to the deep subsurface heat content of the anticyclone.
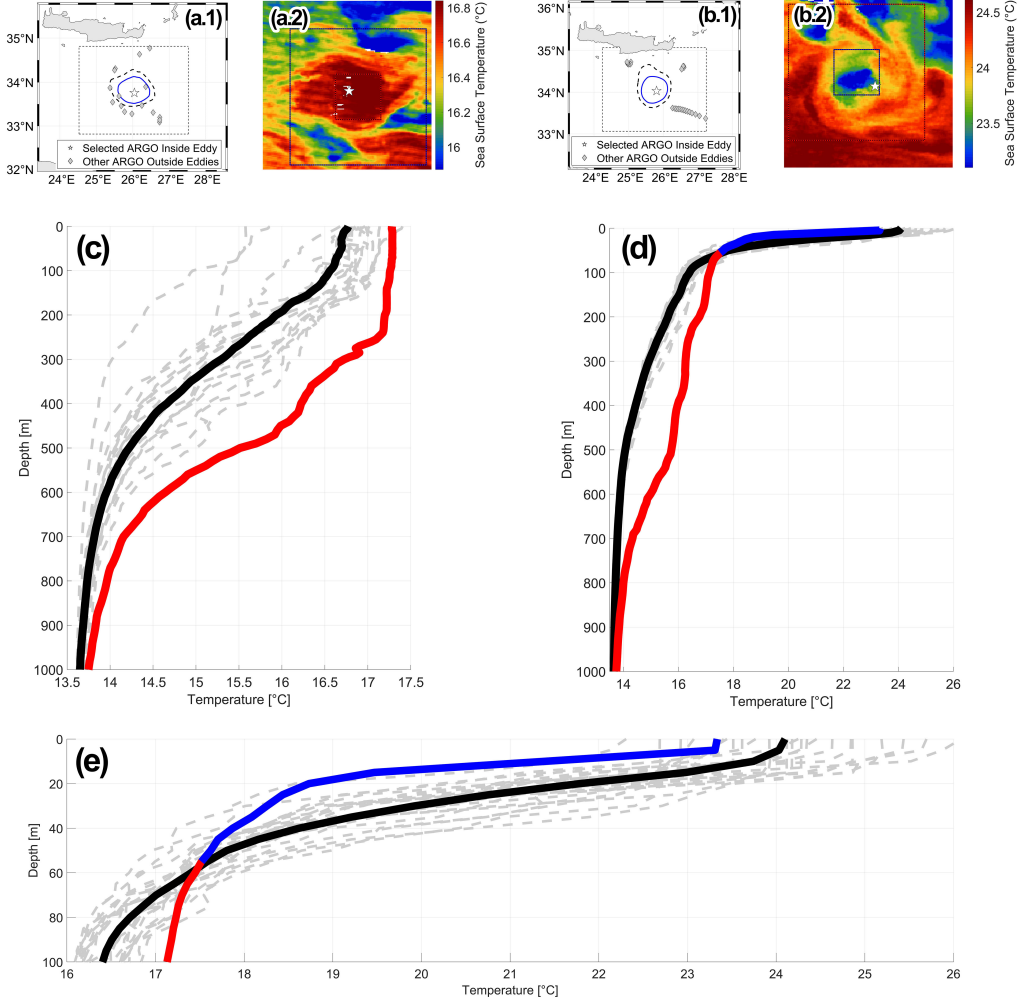
Figure 7. **Seasonal evolution of the vertical structure of the Ierapetra eddy**. Panels (a) and (c) correspond to a warm-core SST observation of the eddy, on 26/07/2017. Panels (b), (d) and (e) correspond to a cold-core SST observation on 26/07/2017. Maps (a.1) and (a.2) show the maximum velocity contour and outermost contour of the eddy, the eddy-sampling ARGO profile with a star and the outside-eddy profiles with diamonds, retained in a region outlined by the dashed rectangle in a period of ± 2 weeks from the eddy observation. Patches (b.1) and (b.2) show the SST signature of the eddy, along with the location of the eddy-sampling profile, plotted with a star. Vertical plots (c), (d) and (e) show the outside-eddy profiles plotted with dashed gray lines and their mean outside-eddy profile with a thick black line. The eddy-sampling profile is plotted with a thick red (blue) line when it is warmer (colder) than the mean outside-eddy profile. Profile (c) shows the winter regular surface signature, with a warm structure, profile (d) the summer inverse surface signature with a cold surface and a warm subsurface structure, while panel (e) zooms into the 100 first meters of (d) to portray the SST inversion.

5 A mechanism of SST anomaly inversion: Single column simulations

The above individual-eddy viewpoint analysis portrays that the winter mixed layer varies significantly inside long-lived mesoscale eddies, particularly in the core of anticyclones. But is this MLD difference between the core of the eddy and its vicinity sufficient enough to explain the inverse eddy-SSTA that occurs during the spring re-stratification ?

To answer this question, and investigate other hypotheses, we use a simplified 1D model of the vertical advection-diffusion of heat in a stratified water column inside and outside mesoscale eddies. The seasonal forcing of the atmosphere is simulated with a sinusoidal surface temperature flux as $Q = Q_0 sin(2\pi t/365.25)$ ($Q_0 > 0$, positive for ocean heat gain), so that the simulation starts with a temperature flux increasing from zero (corresponding to spring). A value of $Q_0 = 150\,W/m^2$ is chosen as an accurate Mediterranean average of total surface heat flux seasonal cycle, following Pettenuzzo et al. (2010), with a negative (positive) maximum heat flux approximately in December (July). As salinity effects are neglected, the temperature flux is equivalent to the buoyancy flux.

An equal surface heat flux is applied for different temperature profiles corresponding to water columns inside a cyclone, anticyclone and a profile outside an eddy respectively. The simulation starts on the end of the winter period, when the MLD is at its deepest. The initial profiles are described analytically in equation 3, whose parameters are chosen so that the simulated profiles represent average temperature profiles in the Mediterranean sea. These stand for a homogeneous MLD of $Z_{MLD} = 50\,m$ at $T_0 = 16°C$ for a cyclone core, $200\,m$ at $18°C$ for an anticyclone core and $100\,m$ at $17°C$ for the outside-eddy profile. Below the mixed layer, we introduce an exponential decrease (typical thickness $Z_T = 150m$) to a deep ocean value of $T_b = 13.5°C$. The $T(z)$ profiles are plotted on panels (b) and (d) of Figure 8, with a blue, red and black line for the anticyclone, cyclone and outside-eddy profiles respectively.

$$
\begin{aligned}
T(z) &= T_0 && ; \text{if} z > Z_{MLD} \\
T(z) &= T_b + (T_0 - T_b)exp\left(\frac{z - Z_{MLD}}{Z_T}\right) && ; \text{if } z < Z_{MLD}
\end{aligned}
\tag{3}
$$

Vertical profiles are forced by the surface heat flux, and in a one-dimensional space the temperature temporal evolution follows a simple diffusion equation :

$$\frac{\partial T}{\partial t} = \frac{\partial}{\partial z}\left(A(z)\frac{\partial T}{\partial z}\right) \tag{4}$$

We assume a steady turbulent mixing coefficient $A(z)$ which depends only on depth. This vertical mixing profile is set by the equation 5, starting from a surface value A_0 down to a deep ocean value A_{back} with a Gaussian vertical shape, with $Z_T = 150\,m$:

$$A(z) = A_{back} + A_0 e^{-(z/Z_T)^2} \tag{5}$$

We first assume that the vertical mixing profile remains the same in the cyclone, the anticyclone and outside-eddy. The surface value A_0 of $10^{-4}m^2.s^{-1}$ is chosen as a typical value for turbulent mixing in the upper ocean while in the deep ocean the mixing is reduced by two orders of magnitude down to $A_{back} = 1.0 \times 10^{-6}m^2.s^{-1}$, the water kinematic viscosity.
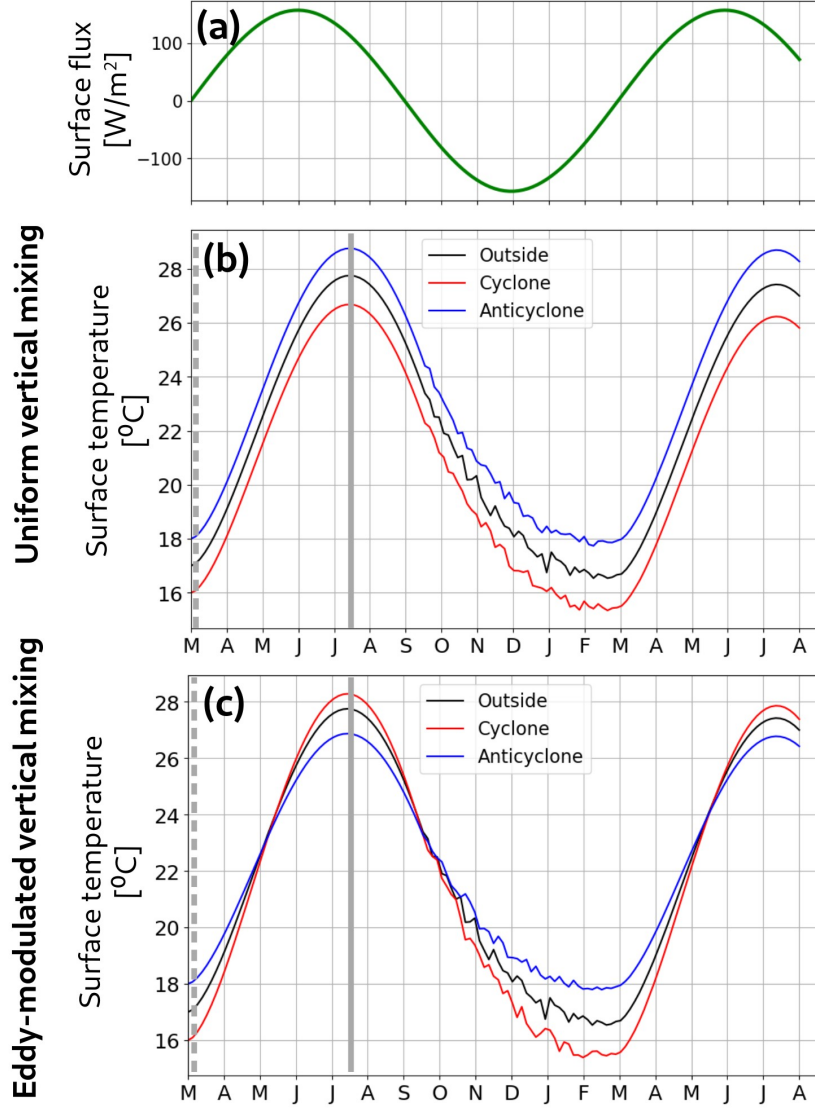
The uniform vertical mixing profile, common for both three water columns, is plotted in panel (a) of Figure 8, while the response of the three water columns (anticyclone, cyclone, outside-eddy) is plotted in panel (b). The simulation starts from a deep-MLD profile at the end of the winter mixing period (dashed line). During spring re-stratification, positive surface is transferred downwards at the same rate for all water columns. As a consequence, the surface temperature difference between the three winter profiles is also maintained in summer (continuous line). This effect is also observed in panel (b) of Figure 9 where the seasonal evolution of the SST of the three water columns, is plotted on a 18-month period. The anticyclonic (cyclonic) profile is constantly warmer (colder) than the outside-eddy profile. A two month lag between the surface flux of Figure 9 panel (a) and the SST of panel (b) is explained through the delay needed for the water column to integrate the radiative forcing.
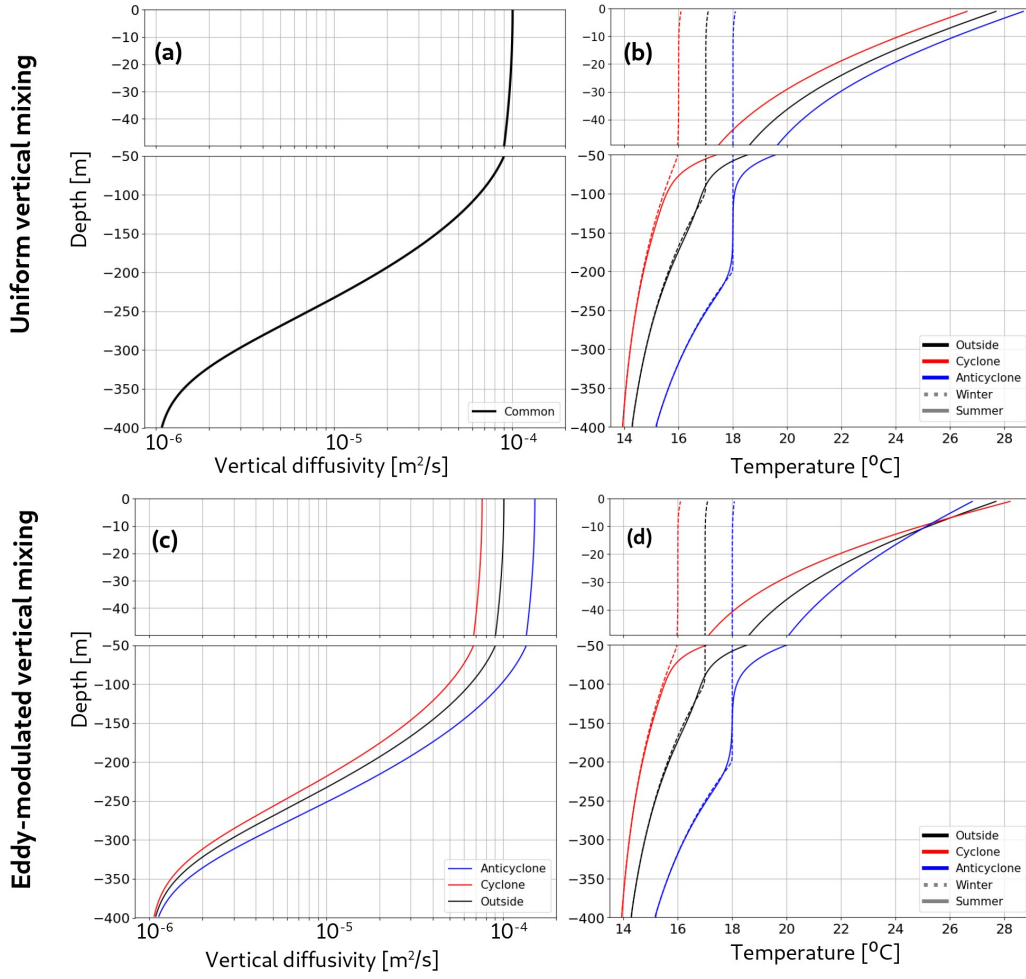
Figure 8. **1D single column experiments : vertical structure**. With a uniform vertical mixing : (a) vertical diffusivity $A(z)$ from equation 5, and (b) temperature profiles in winter (dashed line) and summer (continuous line), corresponding time of the year being reported on Fig.9b . Initial winter profiles are set in equation 3. With eddy-modulated vertical mixing : (c) vertical diffusivity and (d) temperature profiles.

The initial differences of temperature profiles and winter MLD are not sufficient to reproduce observed eddy-SSTA inversion, suggesting that an additional physical process is missing. To explore such a mechanism, we assume that the vertical mixing coefficient is, on the one hand, enhanced in the core of anticyclonic eddies and, on the other hand, reduced in the core of cyclonic eddies. To test this hypothesis, we perform another set of heat vertical diffusion experiment, with the same vertical profiles (equation 3) and

diffusion process (equations 4 and 5), but with a varying surface vertical diffusivity value. A_0 stays outside-eddy at $1.0 \times 10^{-4} \, m^2.s^{-1}$ but is divided by a factor 2 to $5.0 \times 10^{-5} \, m^2.s^{-1}$ in the cyclone profile, and multiplied by 2 to $2.0 \times 10^{-4} \, m^2.s^{-1}$ in the anticyclone one. These eddy-modulated vertical mixing profiles are plotted in panel (c) of Figure 8 with a blue/red/black colour representing the anticyclone/cyclone/outside-eddy profile.

Figure 9. **1D single column experiments : surface temperature**. (a) Surface heat flux forcing the simulation (b) Surface temperature evolution for anticyclone, cyclone and outside-eddy profiles with a uniform vertical mixing and (c) same as (b) but with an eddy-modulated vertical mixing, shown in Fig.8 (c).

Through the season evolution results of the eddy-modulated vertical mixing model, shown in panel (d) of Figure 8, it is observed that heat penetrates deeper in the vertical structure of the anticyclone, resulting in a less stratified profile in summer (blue continuous line). Vice-versa, heat reaches a shallower depth of the cyclone, resulting in a more stratified summer profile (red continuous line). The vertical diffusivity difference is strong enough so that the anticyclone (respectively cyclone) profile gets cooler (warmer) than the outside-eddy profile, resulting in an isotherm crossing similar to what was observed in the Ierapetra anticyclone, seen at panel (e) of Figure 7.

The evolution of surface temperature given by the eddy modulated vertical mixing model, shown in panel (c) of Figure 9 for more than a year and a half, reproduces the same SST anomaly summer inversion in cyclones and anticyclones. The column representative of an AE (CE) core is indeed warmer (colder) in winter at the surface than a column representative of an outside-eddy profile stratification, while turning colder (warmer) in summer, implying that an inverse SST signature has emerged.

These simplified 1D model simulations show that, despite initial differences in vertical stratification or MLD, a differential mixing coefficient, between the core and the periphery of oceanic eddies, is needed to explain the inverse sea surface temperature anomalies and signatures which emerge during the spring re-stratification period.

6 Discussion

The emergence of inverse eddy SST signatures during the summer season, in the global ocean as well as in regional seas, has been well-documented by recent studies (Leyba et al., 2017; Trott et al., 2019; Sun et al., 2019; Liu et al., 2020; Ni et al., 2021). Some of them also link this inversion of eddy surface signature with the spring re-stratification of the ocean surface. This study confirms that such seasonal correlation is also valid for the Mediterranean Sea (Figure 5). Nevertheless, we showcase here that the difference in the MLD alone is a necessary but not sufficient condition for the emergence of an inverse eddy SST signature. We consider thus the hypothesis that eddies modulate the diapycnal mixing in their interior creating a vertical spacing (tightening) of isopycnals in anticyclones (cyclones). Our 1D single column modelling experiment (Figures 8 and 9) shows that a modulation of vertical mixing $A(z)$ inside eddies is needed to reproduce the inversion of the eddy-induced SST anomalies during summer. The origin of this verti-

cal mixing modulation might stem from 3D dynamical processes that cannot be reproduced explicitly in the 1D vertical model.

Some hypotheses exist in the bibliography, and several papers studied the trapping of Near-Inertial Oscillations (NIO) in anticyclones either through a theoretical formulation (Kunze, 1985; Young & Jelloul, 1997), or through modelling experiments (Klein & Smith, 2001; Danioux et al., 2015; Lelong et al., 2020) and observations (Elipot et al., 2010). Enhanced turbulent mixing at depth was also reported when NIO were trapped inside anticyclones (Whalen et al., 2018; Martínez-Marrero et al., 2019). Nevertheless, we are not aware of a theoretical study that provides a direct link between the trapping of NIO and enhanced vertical mixing in the thermocline layer. The opposite trend for cyclones is still under discussion. However, due to the effective Coriolis parameter $f_{eff} = f + \zeta$, which is higher for positive vorticity area ($\zeta > 0$), the spectrum of NIO is expected to be reduced in the core of cyclonic eddies (Kunze, 1985; Young & Jelloul, 1997). This impact of NIO within the eddies is a very plausible explanation of the differential vertical mixing and the observed eddy-SSTA asymmetry between cyclone and anticyclones. Nevertheless, other mechanisms could also be responsible of inverse eddy SST signatures such as nonlinear wind-induced Ekman pumping.

Motivated by the impact of eddies on biological productivity, several studies investigate the self-induced Ekman pumping in the core of mesoscale cyclones and anticyclones. Local currents induced by coherent eddies generate a curl to the surface stress from the relative motion between surface air and water, even if the wind stress is uniform. Hence, an uniform wind applied to an anticyclonic eddy can lead to a divergence and upwelling in its core ((Ledwell et al., 2008), (Gaube et al., 2015),(McGillicuddy Jr, 2016)). A local upwelling could therefore induce a cold core anomaly for anticyclones. However, such a mechanism depends directly on the eddy intensity and we didn't find on the data of this study, any correlation between the amplitude of the temperature anomaly in the core of the eddy and its intensity. Nevertheless, to investigate in more details the impacts of the wind-induced Ekman pumping on the emergence of inverse eddy SST signatures a full 3D numerical simulation will be performed in a future work.

7 Summary and Conclusions

The emergence of inverse eddy SST signatures, in the Mediterranean Sea, is a global seasonal phenomenon that affects all mesoscale eddies. Remote-sensing and in-situ ob-

servations were used to detect and quantify the eddy induced SST anomaly over a 2 years period (2016-2018). We build an eddy core surface temperature index to quantify the amount of Cold Core Anticyclones and Warm Core Cyclones all over the year and especially during the spring re-stratification period. We find that these inverse eddy signatures could reach a peak of 70% in May and June. This seasonal cycle coincides with the seasonal variation of the MLD, both from a statistical point of view, on a basin scale, and from an individual point of view for long-lived eddies. By tracking these eddies we find that some of them alternate several times, from one season to another, between a warm-core and a cold-core SST signature. However, the inverse eddy signatures are constrained to the upper layer of the ocean. For instance, co-localizing ARGO profiles in cold-core anticyclonic eddies reveals that their cold temperature anomaly inversion is limited to the first 50 meters of the ocean, while a warm subsurface anomaly persists deeper.

We propose a simple dynamical mechanism, based on a differential mixing between the eddy core and the surroundings, that leads to reproducing cold-core (warm-core) anticyclones (cyclones) during the spring re-stratification. To do so, we construct a simple vertical column model to compute the impact of the seasonal air-sea flux on the vertical stratification inside and outside eddies. We commence with a winter stratification, with a deep mixed layer, and investigate how the spring re-stratification of the ocean surface differs between the eddy core and its surrounding. By considering only the MLD difference, we were not able to reproduce the inverse eddy-SSTA that were observed during the spring re-stratification. It is only by taking into account a differential diapycnal eddy mixing - increased in anticyclones and diminished in cyclones - that we reproduce correctly the surface temperature inversion in the eddy core, with respect to an outside-eddy profile. This simplified model, suggests that vertical mixing modulation by mesoscale eddies might be the key mechanism that leads to the eddy-SSTA seasonal inversion in the ocean. Besides, even if our study focuses on the Mediterranean Sea, the mechanism proposed here is, a priori, independent of the oceanic region.

Several theoretical studies on near inertial oscillations and corresponding in-situ observations could explain the modulation of the vertical mixing induced by oceanic eddies and the cyclone/anticyclone asymmetry. However, full 3-dimensional modelling are necessary to further investigate these dynamical modes in combination with the wind-induced Ekman pumping inside the eddy core. Such high-resolution simulations are beyond the scope of this study and consist the perspectives of a future work.

This study showcases that a detailed analysis of remote sensing observations of the complex eddy signature at the ocean surface could reveal its subsurface structure in the first tens of meters. This would provide valuable information on the vertical extension of the mixing layer or the bio-geochemical activity in the euphotic layer.

Acknowledgments

References

Abrahms, B., Scales, K. L., Hazen, E. L., Bograd, S. J., Schick, R. S., Robinson, P. W., & Costa, D. P. (2018). Mesoscale activity facilitates energy gain in a top predator. *Proceedings of the Royal Society B*, *285*(1885), 20181101.

Amitai, Y., Lehahn, Y., Lazar, A., & Heifetz, E. (2010). Surface circulation of the eastern mediterranean levantine basin: Insights from analyzing 14 years of satellite altimetry data. *Journal of Geophysical Research: Oceans*, *115*(C10).

Amores, A., Jordà, G., Arsouze, T., & Le Sommer, J. (2018). Up to what extent can we characterize ocean eddies using present-day gridded altimetric products? *Journal of Geophysical Research: Oceans*, *123*(10), 7220–7236.

Auer, S. J. (1987). Five-year climatological survey of the gulf stream system and its associated rings. *Journal of Geophysical Research: Oceans*, *92*(C11), 11709–11726.

Barboni, A., Lazar, A., Stegner, A., & Moschos, E. (2021). Lagrangian eddy tracking reveals the eratosthenes anticyclonic attractor in the eastern levantine basin. *Ocean Science Discussions*, 1–35.

Baudena, A., Ser-Giacomi, E., D'Onofrio, D., Capet, X., Cotté, C., Cherel, Y., & D'Ovidio, F. (2021). Fine-scale structures as spots of increased fish concentration in the open ocean. *Scientific Reports*, *11*(1), 1–13.

Brach, L., Deixonne, P., Bernard, M.-F., Durand, E., Desjean, M.-C., Perez, E., . . . Ter Halle, A. (2018). Anticyclonic eddies increase accumulation of microplastic in the north atlantic subtropical gyre. *Marine pollution bulletin*, *126*, 191–196.

Chelton, D. B., Schlax, M. G., & Samelson, R. M. (2011). Global observations of nonlinear mesoscale eddies. *Progress in oceanography*, *91*(2), 167–216.

Danioux, E., Vanneste, J., & Bühler, O. (2015). On the concentration of near-inertial waves in anticyclones. *Journal of Fluid Mechanics*, *773*.

Elipot, S., Lumpkin, R., & Prieto, G. (2010). Modification of inertial oscillations by the mesoscale eddy field. *Journal of Geophysical Research: Oceans*, *115*(C9).

Escudier, R., Renault, L., Pascual, A., Brasseur, P., Chelton, D., & Beuvier, J. (2016). Eddy properties in the western mediterranean sea from satellite altimetry and a numerical simulation. *Journal of Geophysical Research: Oceans*, *121*(6), 3990–4006.

Everett, J., Baird, M., Oke, P., & Suthers, I. (2012). An avenue of eddies: Quantifying the biophysical properties of mesoscale eddies in the tasman sea. *Geophysical Research Letters*, *39*(16).

Frenger, I., Gruber, N., Knutti, R., & Münnich, M. (2013). Imprint of southern ocean eddies on winds, clouds and rainfall. *Nature geoscience*, *6*(8), 608–612.

Gaube, P., Chelton, D. B., Samelson, R. M., Schlax, M. G., & O'Neill, L. W. (2015). Satellite observations of mesoscale eddy-induced ekman pumping. *Journal of Physical Oceanography*, *45*(1), 104–132.

Gaube, P., Chelton, D. B., Strutton, P. G., & Behrenfeld, M. J. (2013). Satellite observations of chlorophyll, phytoplankton biomass, and ekman pumping in nonlinear mesoscale eddies. *Journal of Geophysical Research: Oceans*, *118*(12), 6349–6370.

Gaube, P., J. McGillicuddy Jr, D., & Moulin, A. J. (2019). Mesoscale eddies modulate mixed layer depth globally. *Geophysical Research Letters*, *46*(3), 1505–1512.

Gómez, G. S. D., Nagai, T., & Yokawa, K. (2020). Mesoscale warm-core eddies drive interannual modulations of swordfish catch in the kuroshio extension system. *Frontiers in Marine Science*.

Hamad, N., Millot, C., & Taupier-Letage, I. (2006). The surface circulation in the eastern basin of the mediterranean sea. *Scientia Marina*, *70*(3), 457–503.

Hausmann, U., & Czaja, A. (2012). The observed signature of mesoscale eddies in sea surface temperature and the associated heat transport. *Deep Sea Research Part I: Oceanographic Research Papers*, *70*, 60–72.

Ioannou, A., Stegner, A., Le Vu, B., Taupier-Letage, I., & Speich, S. (2017). Dynamical evolution of intense ierapetra eddies on a 22 year long period. *Journal*

of Geophysical Research: Oceans, *122*(11), 9276–9298.

Ioannou, A., Stegner, A., Tuel, A., Levu, B., Dumas, F., & Speich, S. (2019). Cyclostrophic corrections of aviso/duacs surface velocities and its application to mesoscale eddies in the mediterranean sea. *Journal of Geophysical Research: Oceans*, *124*(12), 8913–8932.

Klein, P., & Lapeyre, G. (2009). The oceanic vertical pump induced by mesoscale and submesoscale turbulence. *Annual review of marine science*, *1*, 351–375.

Klein, P., & Smith, S. L. (2001). Horizontal dispersion of near-inertial oscillations in a turbulent mesoscale eddy field. *Journal of marine research*, *59*(5), 697–723.

Kunze, E. (1985). Near-inertial wave propagation in geostrophic shear. *Journal of Physical Oceanography*, *15*(5), 544–565.

Laxenaire, R., Speich, S., Blanke, B., Chaigneau, A., Pegliasco, C., & Stegner, A. (2018). Anticyclonic eddies connecting the western boundaries of indian and atlantic oceans. *Journal of Geophysical Research: Oceans*, *123*(11), 7651–7677.

Laxenaire, R., Speich, S., & Stegner, A. (2019). Evolution of the thermohaline structure of one agulhas ring reconstructed from satellite altimetry and argo floats. *Journal of Geophysical Research: Oceans*, *124*(12), 8969–9003.

Laxenaire, R., Speich, S., & Stegner, A. (2020). Agulhas ring heat content and transport in the south atlantic estimated by combining satellite altimetry and argo profiling floats data. *Journal of Geophysical Research: Oceans*, *125*(9), e2019JC015511.

Ledwell, J. R., McGillicuddy Jr, D. J., & Anderson, L. A. (2008). Nutrient flux into an intense deep chlorophyll layer in a mode-water eddy. *Deep Sea Research Part II: Topical Studies in Oceanography*, *55*(10-13), 1139–1160.

Lelong, M.-P., Cuypers, Y., & Bouruet-Aubertot, P. (2020). Near-inertial energy propagation inside a mediterranean anticyclonic eddy. *Journal of Physical Oceanography*, *50*(8), 2271–2288.

Le Vu, B., Stegner, A., & Arsouze, T. (2018). Angular momentum eddy detection and tracking algorithm (ameda) and its application to coastal eddy formation. *Journal of Atmospheric and Oceanic Technology*, *35*(4), 739–762.

Lévy, M., Franks, P. J., & Smith, K. S. (2018). The role of submesoscale currents in structuring marine ecosystems. *Nature communications*, *9*(1), 1–16.

Leyba, I. M., Saraceno, M., & Solman, S. A. (2017). Air-sea heat fluxes associated to mesoscale eddies in the southwestern atlantic ocean and their dependence on different regional conditions. *Climate Dynamics*, *49*(7-8), 2491–2501.

Liu, Y., Yu, L., & Chen, G. (2020). Characterization of sea surface temperature and air-sea heat flux anomalies associated with mesoscale eddies in the south china sea. *Journal of Geophysical Research: Oceans*, *125*(4), e2019JC015470.

Martínez-Marrero, A., Barceló-Llull, B., Pallàs-Sanz, E., Aguiar-González, B., Estrada-Allis, S. N., Gordo, C., . . . Arístegui, J. (2019). Near-inertial wave trapping near the base of an anticyclonic mesoscale eddy under normal atmospheric conditions. *Journal of Geophysical Research: Oceans*, *124*(11), 8455–8467.

Mazloff, M. R., Heimbach, P., & Wunsch, C. (2010). An eddy-permitting southern ocean state estimate. *Journal of Physical Oceanography*, *40*(5), 880–899.

McGillicuddy, D., Robinson, A., Siegel, D., Jannasch, H., Johnson, R., Dickey, T., . . . Knap, A. (1998). Influence of mesoscale eddies on new production in the sargasso sea. *Nature*, *394*(6690), 263–266.

McGillicuddy Jr, D. J. (2016). Mechanisms of physical-biological-biogeochemical interaction at the oceanic mesoscale. *Annual Review of Marine Science*, *8*, 125–159.

Menna, M., Poulain, P.-M., Zodiatis, G., & Gertman, I. (2012). On the surface circulation of the levantine sub-basin derived from lagrangian drifters and satellite altimetry data. *Deep Sea Research Part I: Oceanographic Research Papers*, *65*, 46–58.

Millot, C. (1985). Some features of the algerian current. *Journal of Geophysical Research: Oceans*, *90*(C4), 7169–7176.

Mkhinini, N., Coimbra, A. L. S., Stegner, A., Arsouze, T., Taupier-Letage, I., & Béranger, K. (2014). Long-lived mesoscale eddies in the eastern mediterranean sea: Analysis of 20 years of aviso geostrophic velocities. *Journal of Geophysical Research: Oceans*, *119*(12), 8603–8626.

Moschos, E., Schwander, O., Stegner, A., & Gallinari, P. (2020). Deep-sst-eddies: A deep learning framework to detect oceanic eddies in sea surface temperature images. In *Icassp 2020-2020 ieee international conference on acoustics, speech and signal processing (icassp)* (pp. 4307–4311).

Moschos, E., Stegner, A., Schwander, O., & Gallinari, P. (2020). Classification of eddy sea surface temperature signatures under cloud coverage. *IEEE Journal of Selected Topics in Applied Earth Observations and Remote Sensing*.

Moutin, T., & Prieur, L. (2012). Influence of anticyclonic eddies on the biogeochemistry from the oligotrophic to the ultraoligotrophic mediterranean (boum cruise). *Biogeosciences*, *9*(10), 3827–3855.

Nardelli, B. B., Tronconi, C., Pisano, A., & Santoleri, R. (2013). High and ultra-high resolution processing of satellite sea surface temperature data over southern european seas in the framework of myocean project. *Remote Sensing of Environment*, *129*, 1–16.

Ni, Q., Zhai, X., Jiang, X., & Chen, D. (2021). Abundant cold anticyclonic eddies and warm cyclonic eddies in the global ocean. *Journal of Physical Oceanography*, *51*(9), 2793–2806.

Pessini, F., Olita, A., Cotroneo, Y., & Perilli, A. (2018). Mesoscale eddies in the algerian basin: do they differ as a function of their formation site? *Ocean Science*, *14*(4).

Pettenuzzo, D., Large, W., & Pinardi, N. (2010). On the corrections of era-40 surface flux products consistent with the mediterranean heat and water budgets and the connection between basin surface total heat flux and nao. *Journal of Geophysical Research: Oceans*, *115*(C6).

Stegner, A., Le Vu, B., Dumas, F., Ghannami, M. A., Nicolle, A., Durand, C., & Faugere, Y. (2021). Cyclone-anticyclone asymmetry of eddy detection on gridded altimetry product in the mediterranean sea. *Journal of Geophysical Research: Oceans*, *126*(9), e2021JC017475.

Su, Z., Wang, J., Klein, P., Thompson, A. F., & Menemenlis, D. (2018). Ocean submesoscales as a key component of the global heat budget. *Nature communications*, *9*(1), 1–8.

Sun, W., Dong, C., Tan, W., & He, Y. (2019). Statistical characteristics of cyclonic warm-core eddies and anticyclonic cold-core eddies in the north pacific based on remote sensing data. *Remote Sensing*, *11*(2), 208.

Trott, C. B., Subrahmanyam, B., Chaigneau, A., & Roman-Stork, H. L. (2019). Eddy-induced temperature and salinity variability in the arabian sea. *Geophysical Research Letters*, *46*(5), 2734–2742.

Whalen, C. B., MacKinnon, J. A., & Talley, L. D.   (2018).   Large-scale impacts of the mesoscale environment on mixing from wind-driven internal waves.   *Nature Geoscience*, *11*(11), 842–847.

Young, W., & Jelloul, M. B. (1997). Propagation of near-inertial oscillations through a geostrophic flow. *Journal of marine research*, *55*(4), 735–766.

Zhang, Z., Wang, W., & Qiu, B.   (2014).   Oceanic mass transport by mesoscale eddies. *Science*, *345*(6194), 322–324.